Energy dependence and surface contribution of the folding-model optical potential for nucleon-nucleus scattering at energies up to 1 GeV/nucleon

H. M. Maridi*

Alternative Energy Technology Department, Faculty of Engineering, Philadelphia University, 19392, Jordan and Physics Department, Faculty of Applied Science, Taiz University, Taiz, Yemen

(Received 24 January 2019; revised manuscript received 10 April 2019; published 24 July 2019)

An energy-dependent microscopic optical model potential (OP) is presented to analyze the elastic scattering of protons with incident energies up to 1000 MeV/nucleon on ^{9}Be nucleus. This microscopic optical model is built from the single-folding optical model. The density- and isospin-dependent M3Y-Paris nucleon-nucleon (NN) interaction is used for the real and spin-orbit parts and the NN-scattering amplitude of the high-energy approximation for the imaginary one. The microscopic complex spin-orbit OP is taken within Breiva-Rook approximation. The partial-wave expansion analysis with this optical model potential fails to reproduce the differential cross-section data at energies larger than 100 MeV/nucleon, a good improvement is obtained by including the surface contribution to the imaginary OP where most of the basic scattering observables are reproduced well at the considered wide energy range. The volume integrals are found to be have interesting energy dependencies and their parametrizations can be used to build an energy-dependent microscopic OP that is used to reproduce the observables at a wide energy range. This study shows that the partial-wave expansion analysis using the folding optical model can be used to analyze the scattering data at high energies as well as at low energies.

DOI: 10.1103/PhysRevC.100.014613

I. INTRODUCTION

In the optical model, the interaction between an incident proton and a nucleus can be represented by a complex mean-field potential, which is used to analyze and reproduce the experimental scattering observables by numerical solving of the Schrödinger equation. The optical model potential (OP) is widely used in direct-reaction theory calculations, which give us much important information about energy spectrum, nuclear shape, and nuclear structure.

The OP has been developed in phenomenological and microscopic approaches. Suitable analytical forms as a Gaussian or Woods-Saxon forms are used in the phenomenological OP, and their parameters are determined by adjustment to the best fit with available experimental data. However, it does not include nuclear structure information. In addition, it cannot give unique values of these parameters and many optical potentials can describe equally well a given set of elastic-scattering data [1,2]. In the microscopic approach such as the Glauber or folding models, the OP is determined from detailed nuclear structure and nucleon-nucleon (NN) effective interaction. Generally, the folding model is considered a successful microscopic model to study the cross-section data of the elastic scattering at low incident energies whereas the Glauber model is suitable for high energies scattering. Although the folding OP depends on the NN interaction and the nuclear matter density but it needs to multiply by a renormalization factor to fit the scattering data. These factors are different for different scattered nuclei and different energies. Early studies, such as Refs. [3–6], refer the reduction of the folding OP to the possible dynamic polarization contributions. Furthermore, it may indicate to the opening of inelastic channels as the energy increases [2].

The energy dependence of the nucleon OP has been studied over the years. The energy parametrizations of the OPs are very important in the nuclear reactions in order to analyze and predict the scattering observables. Several global phenomenological OPs for nucleon-nucleus scattering were performed for intermediate and heavy mass nuclei at energies up to 200 MeV/nucleon, see, for example, Refs. [7–13]. They are useful to predict the nucleon OP when elastic scattering data are not available or cannot be measured as in the case for the unstable, dripline nuclei. For heavy nuclei and low bombarding energies, Refs. [7–13] have shown that the optical model gives a satisfactory description of the elastic scattering of nucleons. The model has not enjoyed equal success in its application to light nuclei. In scattering of light nuclei as $A <$ 24, the phenomenological OPs tend to produce parameters that are different from the standard global values, they are physically dubious and cannot give unique values of their parameters [1,8] and the descriptions of the angular distributions are generally poorer [14]. Light nuclei have the property of low level densities, and hence resonance structure is often present [14,15]. In addition, even at fairly high excitations the density of compound nucleus levels is low for light nuclei and hence the nuclear-structure effects, which the optical model cannot describe, are not sufficiently averaged out. There are so few nucleons in light nuclei that it may not be appropriate to replace the nucleus with a potential having a simple radial

*h.maridi@gmail.com

form such as a Woods-Saxon form [15]. Instead, it is useful to assumed that the nucleus can be regarded as a continuous distribution of nuclear matter to the incident particle.

Recently, the proton elastic scattering of light nuclei (helium, lithium, and beryllium isotopes) was analyzed over an energy range from few MeVs/nucleon to 200 MeV/nucleon [16–21]. The angular distributions for elastic-scattering cross sections and reaction cross sections were calculated using the optical model analysis with the partial-wave expansion method. The OP parts were constructed only from the single-folded potentials and their derivatives. Within the folding model, the M3Y *NN* interaction was used for the real part of the OP and the *NN*-scattering amplitude of the high-energy approximation was used for the imaginary part. The derivatives of the real and volume imaginary parts of the OP were added as spin-orbit and surface-imaginary OPs, respectively. This microscopic OP succeeds to fit well the available data until 100 MeV/nucleon. Above this energy value, some minima appear in the calculated angular distribution of the elastic-scattering cross sections. Instead of using partial-wave expansion method, the eikonal approximation that is based on the Glauber theory was used to analyze the scattering at energies larger than 100 MeV/nucleon, see Ref. [19]. The volume integrals of the OP parts were shown to be have energy and mass dependencies, and they were parameterized in empirical formulas. From these parametrizations, a local energy-dependent (E-dependent) OP can be obtained with parameterized renormalization factors as a functions of energy [18,19,21]. It succussed to reproduce the data at energies up to 100 MeV/nucleon.

In the present work, the study is extended to include a wider energy range up to 1000 MeV/nucleon for the $p + {}^{9}$Be elastic scattering. The cross sections and analyzing powers are calculated by a numerical solving of the Schrödinger equation by means of the optical model with the partial-wave expansion method. The real central OP is calculated using the single-folding OP with the density-, and isospin-dependent M3Y-Paris *NN* interaction [22]. The contributions from isoscalar and isovector parts of the folded OP are taken into account. Furthermore, the complex spin-orbit OP is calculated microscopically within a local approximation that suggested by Brieva and Rook [23] where the radial strength of the spin-orbit components (with the total isospin $T = 0$ and $T = 1$) of the M3Y-Paris interactions is folded with the proton and neutron densities. In addition, the imaginary part of the microscopic proton OP is obtained with folding the target densities with the *NN*-scattering amplitude that given by the so-called high-energy approximation (HEA) model [24–26]. The surface contribution to the imaginary part is included. The most important goal of the present work is to determine the correct energy dependencies of the OP parts and then to present a local energy-dependent microscopic OP with parameterized depths as functions of energy. Another aim is to test the ability of the folding optical model with the partial-wave expansion method to reproduce the scattering data at energies up to 1000 MeV/nucleon. The theoretical approaches are given in Sec. II, while the results of the calculations are presented in Sec. III. A summary and conclusions are given in Sec. IV.

II. THEORETICAL CALCULATION

A. Real OP within the single-folding model

The central proton-nucleus potential within the single-folding approach can be represented in terms of the direct ($V_{\rm D}$) and exchange ($V_{\rm EX}$) parts with isoscalar ($V_{\rm IS}$) and isovector ($V_{\rm IV}$) contributions as [22,27]

$$\begin{aligned} V_F(\mathbf{r}) &= V^{\rm D}(\mathbf{r}) + V^{\rm EX}(\mathbf{r}) \\ &= V^{\rm D}_{\rm IS}(\mathbf{r}) + V^{\rm D}_{\rm IV}(\mathbf{r}) + V^{\rm EX}_{\rm IS}(\mathbf{r}) + V^{\rm EX}_{\rm IV}(\mathbf{r}). \end{aligned} \tag{1}$$

$$V^{\rm D}_{\rm IS(IV)}(\mathbf{r}) = \int [\rho_p(\mathbf{r}') \pm \rho_n(\mathbf{r}')] v^{\rm D}_{00(01)}(\rho, s) d^3r'. \tag{2}$$

$$\begin{aligned} V^{\rm EX}_{\rm IS(IV)}(\mathbf{r}) = \int & [\rho_p(\mathbf{r}, \mathbf{r}') \pm \rho_n(\mathbf{r}, \mathbf{r}')] v^{\rm EX}_{00(01)}(\rho, s) \\ & \times j_0(k(E, r)s) d^3r'. \end{aligned} \tag{3}$$

where the $+ve$ sign is related to the isoscalar and $-ve$ sign to the isovector. The isovector part of the folding OP is also known as symmetry potential. $s = |\mathbf{r}' - \mathbf{r}|$ is the distance between the proton and the nucleon in the target and $\mathbf{r}$ is the vector joining the center-of-mass of the incident proton and the target. $\rho_{p(n)}(\mathbf{r}, \mathbf{r}')$ is the one-body density matrix for the protons(neutrons) in the target nucleus with $\rho_{p(n)}(\mathbf{r}) \equiv \rho_{p(n)}(\mathbf{r}, \mathbf{r})$. $k(E, r)$ is the local momentum of the relative motion determined as [28]

$$k^2(E, r) = \frac{2\mu}{\hbar^2}[E_{\rm c.m.} - V_F(r) - V_C(r)], \tag{4}$$

where μ is the nucleon reduced mass, $E_{\rm c.m.}$ is the center-of-mass energy, $V_F(r)$ and $V_C(r)$ are the total nuclear and Coulomb potentials, respectively.

In this work, the M3Y effective *NN* interaction that based on the G-matrix calculations is used. It has two different kinds, namely the Paris [29] and the Reid *NN* interactions [30]. The radial strengths of isoscalar and isovector components for the direct and exchange parts, $v^{\rm D(EX)}_{00}$ and $v^{\rm D(EX)}_{01}$, are defined in terms of three Yukawa [29,30] as

$$v^{\rm D(EX)}_{00(01)}(s) = \sum_{\nu=1}^{3} Y^{\rm D(EX)}_{00(01)}(\nu) \frac{\exp(-R_\nu s)}{R_\nu s}. \tag{5}$$

In the present work, the M3Y-Paris interaction is used and their explicit Yukawa strengths are tabulated in Table I.

To reproduce the basic nuclear matter properties as well as the density and energy dependencies of the nucleon OP, the *NN* interaction considers the density dependencies as [31]

$$v^{\rm D(EX)}(\rho, s) = F(\rho) v^{\rm D(EX)}(s). \tag{6}$$

In the present study, we use the explicit density dependencies that were introduced in Ref. [4,22] for the CDM3Y6 effective Paris potential as

$$F(\rho) = C[1 + \alpha e^{-\beta\rho(\mathbf{r})} - \gamma\rho(\mathbf{r})], \tag{7}$$

where $C = 0.2658$, $\alpha = 3.8033$, $\beta = 1.4099$ fm^3, and $\gamma = 4.0$ fm^3.

In this work, we use the microscopic density distributions for ^{9}Be that are obtained from the Green's function Monte Carlo (GFMC) method using a realistic Hamiltonian containing the Argonne v18 (AV18) two-nucleon potential alone or

TABLE I. Yukawa strengths of the direct and exchange components of the M3Y-Paris interaction [27,29].

ν	R_ν (fm^{-1})	$Y_{00}^{\rm D}(\nu)$ (MeV)	$Y_{01}^{\rm D}(\nu)$ (MeV)	$Y_{00}^{\rm EX}(\nu)$ (MeV)	$Y_{01}^{\rm EX}(\nu)$ (MeV)	$Y_{LS}^{(0)}(\nu)$ (MeV)	$Y_{LS}^{(1)}(\nu)$ (MeV)
1	4.0	11061.625	313.625	−1524.25	−4118.0	−5101.0	−1897.0
2	2.5	−2537.5	223.5	−518.75	1054.75	−337.0	−632.0
3	0.7072	0.0	0.0	−7.8474	2.6157	0.0	0.0

with Illinois model (IL12) [32]. Khoa *et al.* [22,27,31] suggest that the original M3Y *NN* interaction must be multiplied by an energy-dependent factor $g(E)$ in order to account for the empirical energy dependence of the nucleon optical potential. They found that the empirical phenomenological formula $g(E) \simeq 1 - 0.003E$ for M3Y-Paris *NN* interaction is the most adequate in reproducing the data of nucleus-nucleus scattering at energies up to 100 MeV/nucleon [22,27,31] where E is the bombarding energy per nucleon. By using the formula $g(E) \simeq 1 - 0.003E$, the depth of real potential within the folding model is changing sign around 333 MeV/nucleon. The question here is about the possibility to used this formula for energies up to 1 GeV/nucleon. Then, we put $g(E) = 1$ in order to avoid the changing sign of the folding potential and to get the net energy dependence of the optical potentials those fit the scattering data.

For the density matrix, the realistic local approximation proposed in Refs. [28,33] is used

$$\rho_q(\mathbf{r}, \mathbf{r}+\mathbf{s}) \simeq \rho_q\Big(\mathbf{r}+\frac{\mathbf{s}}{2}\Big)\hat{j}_1\Big(k_F^q\Big(\Big|\mathbf{r}+\frac{\mathbf{s}}{2}\Big|\Big)s\Big) \equiv f_q\Big(\mathbf{r}+\frac{\mathbf{s}}{2}\Big), \quad q \equiv p, n, \tag{8}$$

where $\hat{j}_1(x) = 3j_1(x)/x = 3(\sin x - x\cos x)/x^3$. The local Fermi momentum $k_F(r)$ is defined as [33]

$$k_F^q(r) = \left\{\frac{5}{3\rho_q(r)}\left[\tau_q(r) - \frac{1}{4}\nabla^2\rho_q(r)\right]\right\}^{1/2}. \tag{9}$$

The kinetic energy density $\tau(r)$ can be approximated by the extended Thomas-Fermi approximation [26,34,35] as

$$\frac{\tau(\rho)}{2} \simeq \tau_q(\rho_q) = \frac{3}{5}(3\pi^2)^{2/3}[\rho_q(r)]^{5/3} + \frac{C_S|\nabla\rho_q(r)|^2}{\rho_q(r)} + \frac{\nabla^2\rho_q(r)}{3}, \tag{10}$$

valid for each kind of particles $q = n, p$. C_S is the strength of the so-called Weizsäcker term representing the surface contribution to τ. For a finite fermionic system, the commonly accepted value of the Weizsäcker term is $C_S = 1/36$ [34].

The local Fermi momentum $k_F(r)$ then can be written as

$$k_F^q(r) = \left\{[3\pi^2\rho_q(r)]^{2/3} + \frac{5C_S|\nabla\rho_q(r)|^2}{3\rho_q^2(r)} + \frac{5\nabla^2\rho_q(r)}{36\rho_q(r)}\right\}^{1/2}. \tag{11}$$

Then, the direct and exchange parts of the proton-nucleus potential [Eqs. (2) and (3)] can be obtained as

$$V_{\rm IS(IV)}^{\rm D}(\mathbf{r}) = \int [\rho_p(\mathbf{r}') \pm \rho_n(\mathbf{r}')]F\big(\rho(\mathbf{r}')\big)v_{00(01)}^{\rm D}(s)d^3s, \tag{12}$$

and

$$V_{\rm IS(IV)}^{\rm EX}(\mathbf{r}) = \int \left[f_p\Big(\mathbf{r}+\frac{\mathbf{s}}{2}\Big) \pm f_n\Big(\mathbf{r}+\frac{\mathbf{s}}{2}\Big)\right]F\left[\rho\Big(\mathbf{r}+\frac{\mathbf{s}}{2}\Big)\right] \times v_{00(01)}^{\rm EX}(s)j_0[k(E,r)s]d^3s. \tag{13}$$

The spherical potential is radial for the elastic scattering. Therefore, the direct part of the central elastic potential [Eq. (12)] can be obtained in the following form:

$$V_{\rm IS(IV)}^{\rm D}(r) = \frac{}{2\pi^2}\int_0^\infty A_{\rm IS(IV)}(q)v_{00(01)}^{\rm D}(q)j_0(qr)q^2dq, \tag{14}$$

where $v_{00(01)}^{\rm D}(q)$ is the Fourier transform of the direct interaction $v_{00(01)}^{\rm D}(s)$ and $A_{\rm IS(IV)}(q)$ is the Fourier transform of the density profile. They are given by

$$v_{00(01)}^{\rm D}(q) = 4\pi\int_0^\infty v_{00(01)}^{\rm D}(r)j_0(qr)r^2dr, \tag{15}$$

$$A_{\rm IS(IV)}(q) = 4\pi\int_0^\infty [\rho_p(r) \pm \rho_n(r)]F[\rho(r)]j_0(qr)r^2dr. \tag{16}$$

Similarly, the exchange part of the elastic potential [Eq. (13)] can be evaluated as

$$V_{\rm IS(IV)}^{\rm EX}(r) = 2\pi\int_0^\infty G_{\rm IS(IV)}(r,s)v_{00(01)}^{\rm EX}(s)j_0[k(E,r)s]s^2ds, \tag{17}$$

where

$$G_{\rm IS(IV)}(r,s) = \int_{-1}^{1}[f_p(y(x),s) \pm f_n(y(x),s)]F[\rho(y(x)]dx, \tag{18}$$

where $f_q(y,s) = \rho_q(y)\hat{j}_1[k_F^q(y)s]$ with $q \equiv p, n$ and $y(x) = \sqrt{r^2 + \frac{s^2}{4} + rsx}$. $V^{\rm EX}(r)$ includes $k(E,r)$ which is expressed by $V_F = V^{\rm D} + V^{\rm EX}$ as in Eq. (4). So, the self-consistent (local) exchange potential is calculated by an iterative procedure [35].

B. Spin-orbit potential using Brieva and Rook approximation

The spin-orbit part of the nucleon-nucleus optical potential $V_{\rm LS}(r)(\mathbf{L}.\sigma)$ can be evaluated microscopically within the folding model using the two-body spin-orbit *NN* interaction and the nuclear density of the target. The $\mathbf{L}.\sigma = 2\mathbf{L}.\mathbf{S}$ product, which can be given as

$$\mathbf{L}.\sigma \equiv \tfrac{1}{2}[(\mathbf{r}_i - \mathbf{r}_j) \times (\mathbf{p}_i - \mathbf{p}_j)].(\sigma_i + \sigma_j) \tag{19}$$

In the present work, the local approximation that is developed by Brieva and Rook [23] is used to evaluate $V_{\rm LS}(r)$ using the spin-orbit component of the CDM3Y6 interaction. For simplicity, the spin-orbit part of the CDM3Y6 interaction is assumed to has the same density dependence as the central part (6)

$$v_{\rm LS}(\rho, s) = F(\rho) v_{\rm LS}(s). \tag{20}$$

The radial strength of the spin-orbit components (with the total isospin $T = 0$ and $T = 1$) of the M3Y-Paris interaction [29] can also be obtained in terms of Yukawa strengths

$$v_{\rm LS}^{(T)}(s) = \sum_{\nu=1}^{3} Y_{\rm LS}^{(T)}(\nu) \frac{\exp(-R_\nu s)}{R_\nu s}, \tag{21}$$

with the explicit Yukawa strengths tabulated in Table I.

Then, $V_{\rm LS}(r)$ using the spin-orbit component of the CDM3Y6 interaction with including the isospin dependence (20), (21) can be given as

$$V_{\rm LS}(r) = -\frac{F[\rho(r)]}{3}\left[\Phi_p(E, r)\frac{1}{r}\frac{d\rho^p(r)}{dr} + \Phi_n(E, r)\frac{1}{r}\frac{d\rho^n(r)}{dr}\right], \tag{22}$$

$$\Phi_p(E, r) = \int_0^\infty v_{\rm LS}^{(1)}(s)[1 + \hat{j}_1(k(E, r)s)]s^4 ds,$$

$$\Phi_n(E, r) = \frac{1}{2}\int_0^\infty \left\{v_{\rm LS}^{(1)}(s)[1 + \hat{j}_1(k(E, r)s)] + v_{\rm LS}^{(0)}(s)[1 - \hat{j}_1(k(E, r)s)]\right\}s^4 ds. \tag{23}$$

C. Imaginary optical potential within the high-energy approximation

The imaginary part of the OP can be calculated within the HEA model that was derived in Ref. [24,25] on the basis of the eikonal phase inherent in the optical limit of the Glauber theory [36]. It constructed by folding the NN-scattering amplitude with the density of the scattered nucleus. The hybrid potential using the HEA imaginary potential instantaneously with the real folding potential V_F is used to study the proton elastic scattering of light nuclei at energies below 100 MeV/nucleon, recently [16–19,21,26,37–39]. It succeeds to fit the cross-section data at these energies. Within the HEA model, the imaginary OP is expressed as [24–26]

$$W_H(r) = -\frac{\hbar v}{(2\pi)^2}\bar{\sigma}_{NN}\int_0^\infty dq q^2 j_0(qr)\rho(q) f_{NN}(q), \tag{24}$$

where v is the velocity of the nucleon-nucleus relative motion, $\rho(q)$ is the form factor corresponding to the pointlike nucleon density distribution of the nucleus, and $f_{NN}(q)$ is the amplitude of the NN scattering, which can be specified in the form of a Gaussian function [24,40],

$$f_{NN}(q) = \exp\left(-q^2 r_0^2/4\right), \tag{25}$$

where $r_0^2 = 0.439$ fm^2 [40] is the range parameter. $\bar{\sigma}_{NN}$ is the average over isospin total NN cross section. It has been parameterized in Refs. [40,41] as a function of energy,

$$\bar{\sigma}_{NN} = \frac{N_P N_T \sigma_{nn} + Z_P Z_T \sigma_{pp} + (Z_P N_T + N_P Z_T)\sigma_{np}}{A_P A_T}. \tag{26}$$

The pp and nn cross sections are given in (fm^2) by

$$\sigma_{pp} = \sigma_{nn} = (1.373 - 1.504\beta^{-1} + 0.876\beta^{-2} + 6.867\beta^2), \tag{27}$$

where

$$\beta = \frac{\upsilon}{c} = \sqrt{1 - \left(\frac{m}{E_N + m}\right)^2} \tag{28}$$

is the ratio of the relative to the light velocities, $E_N = E/A$ is the incident energy per nucleon (in MeV), and $m = 931.494$ MeV. For the np cross section, σ_{np} is expressed in two forms as:

$$\sigma_{np} = -7.067 - 1.818\beta^{-1} + 2.526\beta^{-2} + 11.35\beta. \tag{29}$$

for the energy per nucleon $E_N > 10$ MeV.

For $E_N < 10$ MeV, the following expression that is given by Enge [41,42] is used:

$$\sigma_{np} = \frac{273}{(1 - 0.0553E_N)^2 + 0.35E_N} + \frac{1763}{(1 + 0.334E_N)^2 + 6.8E_N}. \tag{30}$$

D. Total optical potential

The present scattering problem considers a proton with an energy E incident upon a target with a mass number A and scattered by a central spherical optical potential $U_{\rm OP}(r)$ which can be generally written as

$$U_{\rm OP}(r) = V(r) + iW(r) + U_{\rm SO}(r) + V_C(r), \tag{31}$$

where V, W, and $U_{\rm SO}$ are the central real, imaginary, and spin-orbit parts of the OP, respectively. $V_C(r)$ is the Coulomb potential of a uniformly charged sphere of radius $1.2A^{1/3}$.

In the elastic scattering of light nuclei the transfer and breakup processes also take place. Therefore, it is important to include the virtual nonelastic contributions. It is known that at low incident energy an underestimation of angular distributions at backward angles indicates a surface absorption that is too strong [8]. So, the surface imaginary term is included in most of the global phenomenological OPs, it is added usually as a derivative of the Wood-Saxon function [7–9,11–13]. So, the imaginary OP consists of volume and surface absorption components [$W(r) = W_v(r) + W_s(r)$]. The volume imaginary potential is often arranged to simulate the ingoing-wave boundary condition to model loss of flux due to fusion. The surface imaginary accounts for loss of flux due to non-elastic direct reaction channels [43]. For using the

microscopic folding-model potential, inclusion of a surface imaginary term to the OP leads to a better agreement with the experimental data as shown in our previous papers [16–21], as well as in Refs. [37,39,44] for proton-nucleus scattering of light nuclei. It is known from the theory of inelastic scattering that excitations of nuclear collective states can be understood by introducing transition potentials in the form of the derivative of an elastic scattering potential, this contribution can be considered to be the so-called dynamical polarization potential, which allows one to simulate the surface effects and increase the absorption in the surface region and thus, one adds a derivative of the microscopic potential as a surface potential as in Refs. [39,44–46] for nucleon-nucleus OP or Refs. [47,48] for nucleus-nucleus OP.

Most analyses of low-energy scattering and most model calculations are consistent with a spin-orbit potential that is essentially real at $E \leqslant 65$ MeV [12,23]. At energies from 20–200 MeV, from the CH89 analysis of the considered extensive database, there is no evidence for an imaginary component of the spin-orbit potential in a global nucleon-nucleus optical-model potential [12]. A more usual result is that there is no evidence for any imaginary spin-orbit term but many studies at the highest energies found that the fitting of the elastic scattering with an optical-model potential requires a small positive imaginary spin-orbit potential that may be a result of cancelations between components arising from different physical processes [49].

The complex spin-orbit term is inserted to many global phenomenological OPs that are based on the complex proton and neutron spin-orbit potentials vary similarly in depths and radial shapes to fit the nucleon-nucleus scattering data at energies from 1–200 MeV [7,8,50]. In Ref. [51] the imaginary spin-orbit term slightly improves the scattering data of $p+{}^{9}$Be at energies from 100–220 MeV/nucleon. In addition, a simple energy-dependent optical potential of proton scattering from light nuclei in the energy range 50–160 MeV uses a complex spin-orbit potential to fit the data [52,53]. Also, the imaginary spin-orbit potential is included to fit the data of proton elastic scattering at energies from 200–500 MeV/nucleon [54]. Bauge *et al.* [50] use two microscopic spin-orbit potentials based on the derivative of the nuclear matter density that given by Scheerbaum [55], they found that performing optical model calculations up to 200 MeV requires a complex spin-orbit interaction.

In the present calculations, the surface and imaginary spin-orbit contributions to the optical potential are included and the total microscopic optical potential can be written as

$$U_{\rm OP}(r) = N_R V_F(r) + i\left[N_I W_H(r) - N_{\rm IS} r\frac{d}{dr}W_H(r)\right] + \left(N^R_{\rm SO} + iN^I_{\rm SO}\right)V_{\rm LS}(r)\mathbf{L}.\sigma + V_C(r), \quad (32)$$

where V_F [Eq. (1)] is the real OP, which is calculated with the single-folding model using the density- and isospin-dependent M3Y-Paris NN interaction, W_H [Eq. (24)] is the volume imaginary potential using the high-energy approximation model, and $V_{\rm LS}(r)(\mathbf{L}.\sigma)$ [Eq. (22)] is the spin-orbit OP which is constructed microscopically by the local approximation that suggested by Brieva and Rook [23]. As usually used, the derivative of the volume imaginary potential is added as a surface imaginary potential and the imaginary spin-orbit potential is taken similar to the real one.

Most of studies for elastic scattering of light nuclei introduce renormalization factors to the elastic scattering potentials to account all possible virtual couplings between the ground and higher excited states and remove flux from the elastic channel [2,3]. Also, the real and imaginary spin-orbit potentials that are based on Brieva and Rook approximations need large scaling to fit the nucleon scattering data of light nuclei than those of heavy nuclei, see, for example, Ref. [56]. Therefore, the renormalization factors, N_R, N_I, $N_{\rm IS}$, $N^R_{\rm SO}$, and $N^I_{\rm SO}$ are introduced to the real, volume imaginary, surface imaginary, and spin-orbit microscopic potentials, respectively. They are chosen according to the best-fitting procedure. They correspond to the strengths of the Woods-Saxon phenomenological OP. One of the aims of this work is to obtain the energy dependencies of these renormalization factors and then the energy dependence of the OP.

E. Volume integrals

Generally, the volume integrals are relatively invariant functions of the OP parameters and give insight in the behavior of the optical potentials as a function of mass and energy [8]. In addition, they have been used to help in selecting among possible potential families at high energies [2]. Furthermore, the best-fit OPs with different densities or interactions can be having different shapes or renormalization factors, but they must have similar systematic volume integrals for the same reaction [16,17].

Generally, the volume integral per nucleon of the spherical potential, $U(r)$, can be given by

$$J(U) = \frac{1}{A}\int U(r)d^3r = \frac{4\pi}{A}\int U(r)r^2dr. \quad (33)$$

Then, the volume integrals of the real, volume imaginary, spin imaginary, total imaginary, real spin-orbit, and imaginary spin-orbit parts of the OP are denoted correspondingly by J_R, $J_{\rm IV}$, $J_{\rm IS}$, J_I, $J^R_{\rm SO}$, and $J^I_{\rm SO}$. They are defined as

$$J_R = \frac{4\pi}{A}\int [N_R V_F(r)]r^2dr = N_R J(V_F), \quad (34)$$

$$J_{\rm IV} = \frac{4\pi}{A}\int [N_I W_H(r)]r^2dr = N_{\rm IV} J(W_H), \quad (35)$$

$$J_{\rm IS} = \frac{4\pi}{A}\int \left[-N_{\rm IS} r\frac{d}{dr}W_H(r)\right]r^2dr = N_{\rm IS} J[-rdW_H(r)/dr], \quad (36)$$

$$J_I = J_{\rm IV} + J_{\rm IS}, \quad (37)$$

and

$$J^R_{\rm SO} = \frac{4\pi}{A}\int \left[N^R_{\rm SO} V_{\rm LS}(r)\right]r^2dr = N^R_{\rm SO} J(V_{\rm LS}), \quad (38)$$

$$J^I_{\rm SO} = \frac{4\pi}{A}\int \left[N^R_{\rm SO} V_{\rm LS}(r)\right]r^2dr = N^I_{\rm SO} J(V_{\rm LS}). \quad (39)$$

TABLE II. $d\sigma/d\Omega$ data for $p + {}^{9}$Be elastic scattering.

Data	Incident energy (in MeV/nucleon) [Reference]
$d\sigma/d\Omega$	3 [57], 6.0, 10.0 [58], 13 [59], 17, 21, 25 [60], 30.3 [59], 35.2 [61], 46 [62], 49.4 [63], 54.7, 74.7 [51], 100.6 [64], 135 [65], 160 [66], 179.9 [67], 201.4 [68], 220 [69], 317.4 [70], and 497.5 [71], and 1000 [72]
$A_y(\theta)$	7 [73], 8.5 [74], 11.4 [75], 12 [73], 17.8 [76], 30.3 [77], 42 [78], 49.75 [79], 74.7 [51], 100.6 [64], 141.5 [80], 181 [81], 201.4 [68], 317 [70,82], and 1000 [72]

The volume integrals of the original OPs (without renormalizations) are calculated numerically by using of Eq. (33) at each energy and then they are parameterized over the whole energy range as

$$\begin{aligned} J(V_F) &\approx 555.5\exp(-0.00392E) \\ J(W_H) &\approx -212.25 + 0.5239E + \frac{4056.3}{\sqrt{E}} \\ J(-rdW_H(r)/dr) &\approx 3J(W_H) \\ J(V_{\rm LS}) &\approx 26.8 + 8.22\exp(-0.00934E). \end{aligned} \quad (40)$$

Here $J[rdW_H(r)/dr]$ is three times of $J[W_H(r)]$ can be obtained analytically from the known formula of integration by parts, $\int f dg = fg - \int g df$.

F. Method of calculations

In this work, the experimental cross-section and analyzing-power data for $p + {}^{9}$Be elastic scattering at an energy range from 3–1000 MeV/nucleon are considered. They are listed with their references in Table II. In addition, the experimental reaction and total cross sections can be found in Refs. [83,84].

The microscopic optical model potential [Eq. (32)] is used in the calculations of the cross sections. These cross-section data are calculated by numerical solving of the Schrödinger equation by means of the optical model code OPTIM [85].

The best-fit renormalization factors of the OP are determined by a fitting procedure of the scattering observables, which is carried out to achieve minimum χ^2. Furthermore, they must be smooth regarding energy and are chosen according to the standard behaviors of the corresponding volume integrals. The following definition of χ^2 is used:

$$\chi^2 = \frac{1}{N}\sum_{k=1}^{N}\left[\frac{\sigma_{\rm th}(\theta_k) - \sigma_{\rm ex}(\theta_k)}{\Delta\sigma_{\rm ex}(\theta_k)}\right]^2, \quad (41)$$

where $\sigma_{\rm th}(\theta_k)$ and $\sigma_{\rm ex}(\theta_k)$ are the theoretical and experimental cross sections at the angle θ_k, respectively. $\Delta\sigma_{\rm ex}(\theta_k)$ is the experimental error and N is the number of data points. The errors of the experimental data are not provided for most of the considered experimental data, so these errors can be taken as 10% of the corresponding experimental data. In addition, the visual fit must be noted by eye because the minimum χ^2 does not necessarily mean a better visual result in some cases [8]

After the best-fitting procedure, the volume integrals of the best-fit OP parts [Eqs. (34)–(36), (38), and (39)] are parameterized as functions of energies. Then, from the energy parametrizations of the volume integrals, the parameterized N factors of the OP parts can be determined as

$$\begin{aligned} N_R(E) &= \frac{J_R(E)}{J(V_F)} \\ N_{\rm IV}(E) &= \frac{J_{\rm IV}(E)}{J(W_H)} \\ N_{\rm IS}(E) &= \frac{J_{\rm IS}(E)}{J(-rdW_H(r)/dr)} \\ N^R_{\rm SO}(E) &= \frac{J^R_{\rm SO}(E)}{J(V_{\rm LS})} \\ N^I_{\rm SO}(E) &= \frac{J^I_{\rm SO}(E)}{J(V_{\rm LS})}. \end{aligned} \quad (42)$$

So, the optical potential [Eq. (32)] can be rewritten as

$$\begin{aligned} U_{\rm OP}(r,E) &= N_R(E)V_F(r) \\ &+ i\left[N_I(E)W_H(r) - N_{\rm IS}(E)r\frac{d}{dr}W_H(r)\right] \\ &+ \left[N^R_{\rm SO}(E) + iN^I_{\rm SO}(E)\right]V_{\rm LS}(r)\mathbf{L}.\sigma + V_C(r), \end{aligned} \quad (43)$$

The main goal of this study is the determination of the energy dependence of N factors those determine the true energy dependence of optical potentials.

III. RESULTS AND DISCUSSION

A. Cross sections and analyzing powers

In our previous work, the proton elastic scattering of ^{9}Be nucleus was analyzed over energies up to 200 MeV/nucleon using the optical model analysis with the partial-wave expansion method. In the calculation, the hybrid OP [Eq. (32)] except that the real spin-orbit term was taken as a derivative of the real folding OP [18,19,21] and the imaginary spin-orbit potential was not included. The calculation succeeds to fit well the available data until 100 MeV/nucleon. Above this energy value, some minima appear in the calculated angular distribution of the elastic-scattering cross sections.

In the present work, the scattering data of $p + {}^{9}$Be elastic scattering are calculated using the microscopic OP [Eq. (32)] with complex spin-orbit OP that based on the Brieva-Rook approximation. Figure 1 presents the calculated differential cross sections of $p + {}^{9}$Be elastic scattering at energies up to 200 MeV/nucleon in comparison with the two types of the spin-orbit OP. The results with the OP with Brieva-Rook complex spin-orbit potential, which represents this work, are presented in solid lines, and those using the real spin-orbit OP as a derivative of the real OP, which represents our previous

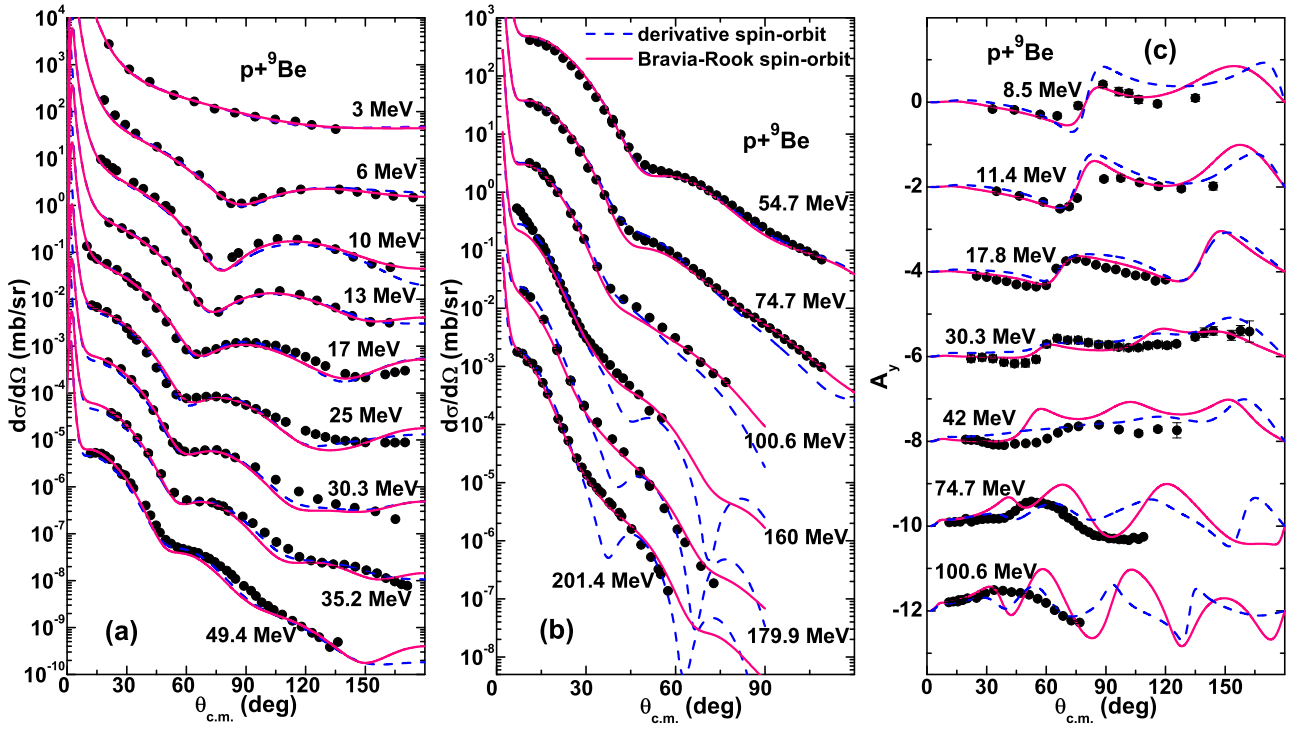

FIG. 1. Differential cross sections and analyzing powers of $p + {}^{9}$Be elastic scattering in comparison with the experimental data. The symbols represent the experimental data at different energies in MeV/nucleon and the lines represent the results of the optical model calculation with the partial-wave expansion method. The solid lines represent the results of calculations using the Brieva-Rook spin-orbit OP. The dashed lines represent the results of calculations using the spin-orbit OP as a derivative of the real folding OP from Ref. [19]. The curves and data points at the top represent true values, while the others are divided by factors of 10, 100, and so on for the differential cross sections. For the polarization calculation, the curves and data points at the top represent true values, while the others by factors of -2, -4, -6, etc. The experimental data are listed in Table II.

work [19], are shown in dashed lines. At low energies, both types of the spin-orbit potential give good agreement with the data. However, at energies larger than 100 MeV/nucleon, the spin-orbit that is based on the derivative of the real folding OP fails to reproduce the whole range of the cross-section and polarization data and two minima appear in the angular distributions. It is clear that the present OP with the Brieva-Rook spin-orbit OP fills these minima and give good agreement with the whole angular range. For the analyzing powers, the data are quite reasonable fitted at low energies but the data at 74.7 and 100.6 Mev/nucleon have not good fits.

The surface contribution to the OP is usually negligible at energies larger than 100 MeV/nucleon. Many studies assumed that the surface absorption is too strong and $W_s(r)$ is dominant at low incident energies whereas the absorption is completely dominated by the volume imaginary OP $W_s(r)$ at higher energies, see for example, Refs. [7,8]. To study the contribution of the surface term of the OP, Fig. 2 presents the calculated differential cross sections and analyzing powers of $p + {}^{9}$Be elastic scattering. The results with the OP without the surface imaginary potential are presented in dashed lines, and those including the surface part are shown in solid lines.

From Figs. 2(a) and 2(b), one can notice that the experimental data of $p + {}^{9}$Be at energies up to 100 MeV/nucleon are reproduced with good fit by using the OP with and without the surface term. In the optical model calculation without including the surface imaginary part, more than one minimum are found in the calculated differential cross sections for the energies larger than 100 MeV/nucleon as shown in Fig. 2(b). At 135 MeV/nucleon, the first minimum is found at around 45° and the second one at about 75°. The angular positions of these minima decrease with an increase in the incident energy. This result is also found in the calculated angular distributions of $p + {}^{4}$He and $p + {}^{6,7}$Li elastic scattering at about 155 MeV/nucleon [17].

Unexpectedly, the scattering data need a large contribution of the surface imaginary OP to get the best fitting. The results reveal that, in the present work, the including of the surface contribution to the OP at high energies improves the results and gives the good agreement with the data over all the angular range; and the minima that appeared in the angular distribution disappeared as shown in Fig. 2(b).

The calculated analyzing powers for $p + {}^{9}$Be elastic scattering are presented in Fig. 2(c). In this figure, the experimental data are presented in comparison with the results of calculations. The A_y data are reproduced well with a good reasonable fit at low energies. At energies larger than 50 MeV/nucleon, the analyzing powers are not in good agreement with the data but at least the structure at forward scattering angles are rather well reproduced and the minima and maxima at the backward scattering angles have larger scale than those of the data.

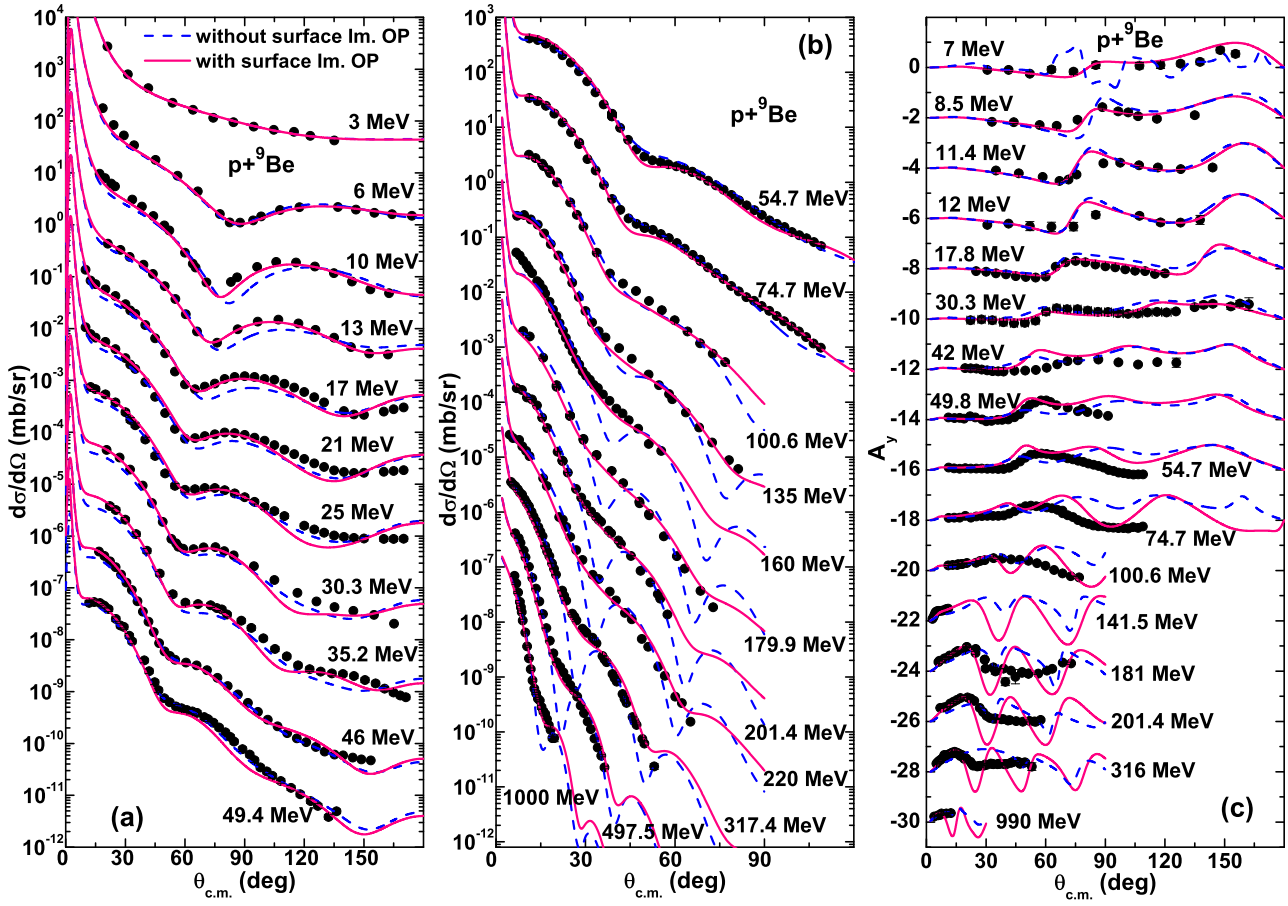

FIG. 2. Differential cross sections and analyzing powers of $p + {}^{9}$Be elastic scattering in comparison with the experimental data. The symbols represent the experimental data at different energies in MeV/nucleon and the lines represent the results of the optical model calculation with the partial-wave expansion method. The solid and dashed lines represent the results of calculations using the microscopic OP [Eq. (32)] with and without surface imaginary part, respectively. For the differential cross sections, the curves and data points at the top represent true values, while the others are divided by factors of 10, 100, and so on. For the polarization calculation, the curves and data points at the bottom represent true values, while the others by factors of -2, -4, -6, etc. The experimental data are listed in Table II.

The total nuclear reaction cross sections (σ_R) are considered important constraints for the choice of the optical potential parameters. In addition, they give information about the radii of the scattering nuclei and their structure.

The calculated reaction (σ_R) and total ($\sigma_{\rm tot}$) cross sections for $p + {}^{9}$Be reaction at different energies using the optical model analysis with the partial-wave expansion are presented in Fig. 3 in comparison with the experimental values [83,84]. It is shown that the calculated values are in agreement with the available experimental data. The σ_R and $\sigma_{\rm tot}$ decrease with an increase of the projectile incident energy up to about 200 MeV/nucleon, and then they increase very slowly with energy up to 1000 MeV/nucleon. In addition, the calculated values of reaction and total cross sections using the OP with the surface imaginary part are found to be slightly larger than that without including the surface potential.

Generally, all the potential parts of the OP are very sensitive at low energies. The real central and spin-orbit potentials are weak and do not have a significant effect at high energies. However, the volume and surface imaginary potentials still have strong effect on the fitting of the data over all energy ranges. The calculations were repeated without considering the imaginary spin-orbit potential and it was found that the fits did not significantly deteriorate.

B. Energy dependencies of the volume integrals

The calculated volume integrals of the OPs for $p + {}^{9}$Be elastic scattering using the optical model analysis are plotted in Fig. 4. The volume integrals of OP parts are calculated using [Eqs. (34)–(39)]. In Figs. 4(a)–4(c), the symbols represent the calculated volume integrals of the best-fit OPs and the lines represent the parameterized volume integrals, which will be discussed later.

From Fig. 4, using the OPs with and without the surface imaginary part give approximately similar volume integrals. However, the calculated values of the $J^R_{\rm SO}$ and $J^I_{\rm SO}$ using the surface potential are found to be slightly greater than those using the OP without the surface potential.

Generally, the volume integrals of the OP parts have systematic behaviors. It is clear from Figs. 4(a) and 4(c) that the J_R and $J^R_{\rm SO}$ increase with energy increasing until they reach a

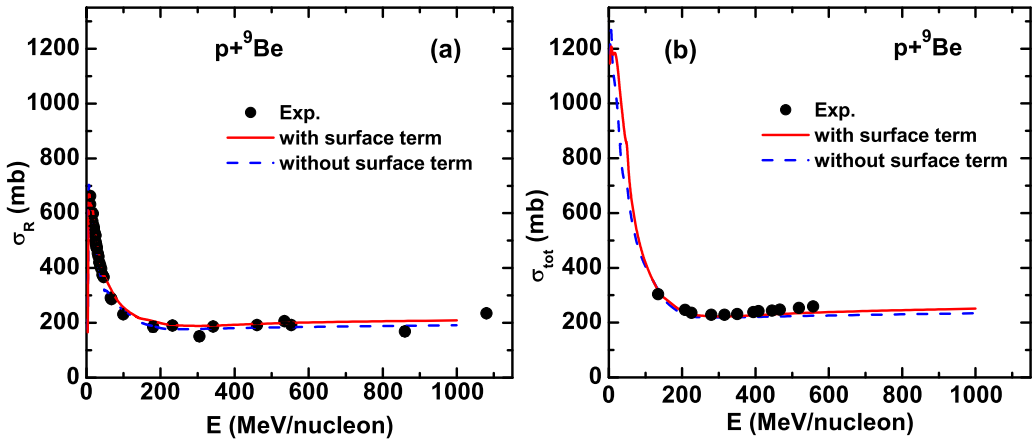

FIG. 3. Calculated σ_R and $\sigma_{\rm tot}$ for the elastic scattering of $p + {}^9$Be. They compared with the available experimental data.

maximum value at a definite energy (denoted by E_R for J_R and $E^R_{\rm SO}$ for $J^R_{\rm SO}$). After that, they begin to decrease exponentially with energy. E_R is found at about 13 MeV/nucleon and $E^R_{\rm SO}$ at about 6 MeV/nucleon.

Different energy parametrizations are used for the depth of the real OP and then J_R, namely: a polynomial form [7,8]; an exponential decay form of Perey and Buck [86], which was used, for example, in Refs. [9,13]; a logarithmic formula [87,88]; and a reciprocal formula [17]. For low energies ($E < E_R$), the rising of the real volume integral J_R was parameterized by a Gaussian formula as in Refs. [89,90]. For the spin-orbit potential, the energy dependence of its depth was parameterized exponentially as in Refs. [7–9,13]. In the present work, it is found that the Gaussian formula for low energies and exponential decay for the other energy range give the best fitting for both J_R and $J^R_{\rm SO}$. The parametrizations and their best-fit parameters of J_R and $J^R_{\rm SO}$ are presented in Table III.

The imaginary volume integrals, J_I, depends strongly on the energy at low energies because many reaction channels open at energies around the Coulomb barrier [91]. The imaginary OP takes into account the absorption of the flux in the nonelastic channels. So, it increases when a new channel is open from below the lowest inelastic channel to a saturation value observed at relatively high energies [90,91].

In the present work, the volume integrals of the volume, surface, and total imaginary OPs have similar behaviors. They begin small at low energies and then increase rapidly up to a maximum value. Thereafter, they decrease linearly and very slowly with increasing energy up to 200 MeV/nucleon. In previous studies that were done for the proton scattering with intermediate and heavy nuclei ($A \geqslant 24$), the calculated imaginary volume integrals were saturated after they reached a maximum, as shown in Refs. [2,9,13]. But the present study for the proton scattering with light nuclei ($A \leqslant 12$) shows that the J_I values decrease slowly after they reach a maximum. For energies larger than 200 MeV/nucleon, it is shown that they increase linearly and strongly with increasing the energy up to 1 GeV/nucleon, see Fig. 4(b).

There are different parametrizations for J_I: the Fermi-like parametrization that was first introduced in Ref. [92] and used in Refs. [12,90,93]; the functional form of Brown and Rho [94] that was successfully applied in Refs. [7,8,13]; and the Jeukenne-Mahaux formula [95], which was applied in Ref. [9]. These formulas suggest that the depth of the volume imaginary OP, and its volume integral saturates at a maximum value at high energies, whereas that of the surface imaginary potential decrease exponentially at high energies. In the present work, the results show that $J_{\rm IV}$ and $J_{\rm IS}$ decrease slowly and linearly with energy after it reaches the maximum

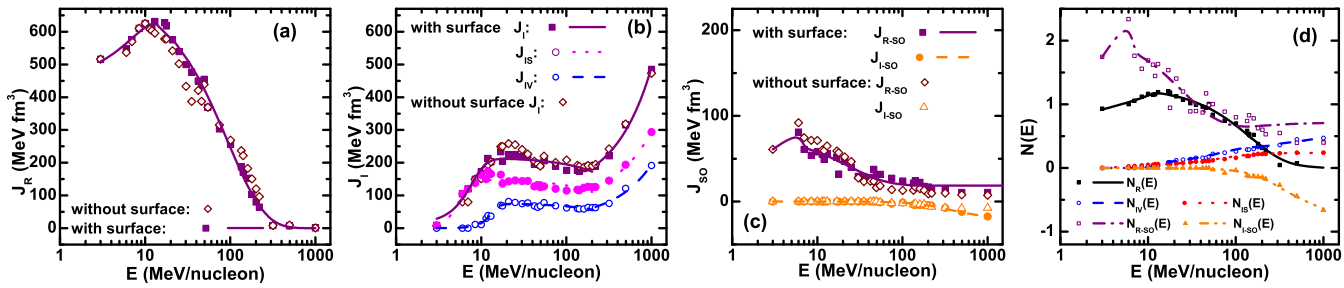

FIG. 4. Dependence of the volume integrals and renormalization factors on the incident energy for the $p + {}^9$Be elastic scattering optical potentials. The microscopic OPs are calculated by Eq. (32). The symbols represent the volume integrals and N factors of the best-fit OP and the lines represent the parameterized volume integrals and N factors as functions of energy. See text for more explanation. The symbols in (a), (b), and (c) represent the calculated volume integrals and the lines represent the parameterized volume integrals as functions of energy. In (d), the symbols represent the best-fitted N factors and the lines represent the parameterized $N(E)$ factors.

TABLE III. Energy parametrizations of the volume integrals of the best-fit OPs for $p + {}^{9}$Be elastic scattering using the optical model calculations. The parameters E and w are given in MeV, η in MeV^{-1}, and J in MeV fm^3.

OP part	Parametrization	Parameters
Real	$J_R(E) = \begin{cases} J_{\rm R}^{(1)} \exp\left[-(E-E_R)^2/w_R^2\right] & \text{for } E \leqslant E_R \\ J_{\rm R}^{(2)} \exp\left(-\eta_R E\right) & \text{for } E \geqslant E_R \end{cases}$	$\begin{cases} J_{\rm R}^{(1)} = 624.0 \quad w_R = 22.12 \\ E_R = 13 \\ J_{\rm R}^{(2)\rm a} = 721.3 \quad \eta_R = 0.0107 \end{cases}$
Volume Imaginary	$J_{\rm IV}(E) = \begin{cases} \frac{J_{\rm IV}^{(1)} - \eta_{\rm IV}^{(1)} E}{1+\exp\left(E_{\rm IV}-E\right)/w_{\rm IV}} & \text{for } E \leqslant 200 \text{ MeV} \\ J_{\rm IV}^{(2)} + \eta_{\rm IV}^{(2)} E & \text{for } E \geqslant 200 \text{ MeV}. \end{cases}$	$\begin{cases} J_{\rm IV}^{(1)} = 76.7 \quad \eta_{\rm IV}^{(1)} = 0.0977 \\ E_{\rm IV} = 12.5 \quad w_{\rm IV} = -1.84 \\ J_{\rm IV}^{(2)\rm a} = 28.4 \quad \eta_{\rm IV}^{(2)} = 0.1663 \end{cases}$
Surface Imaginary	$J_{\rm IS}(E) = \begin{cases} \frac{J_{\rm IS}^{(1)} - \eta_{\rm IS}^{(1)} E}{1+\exp\left(E_{\rm IS}-E\right)/w_{\rm IS}} & \text{for } E \leqslant 200 \text{ MeV} \\ J_{\rm IS}^{(2)} + \eta_{\rm IS}^{(2)} E & \text{for } E \geqslant 200 \text{ MeV}. \end{cases}$	$\begin{cases} J_{\rm IS}^{(1)} = 150.0 \quad \eta_{\rm IS}^{(1)} = 0.1960 \\ E_{\rm IS} = 5.33 \quad w_{\rm IS} = -0.94 \\ J_{\rm IS}^{(2)\rm a} = 80.2 \quad \eta_{\rm IS}^{(2)} = 0.2155 \end{cases}$
Real Spin-orbit	$J_{\rm SO}^R(E) = \begin{cases} J_{\rm SO}^{(R1)} \exp\left[-(E-E_{\rm SO}^R)^2/{w_{\rm SO}^R}^2\right] & \text{for } E \leqslant E_{\rm SO}^R \\ A + J_{\rm SO}^{(R2)} \exp\left(-\eta_{\rm SO}^R E\right) & \text{for } E \geqslant E_{\rm SO}^R \end{cases}$	$\begin{cases} E_{\rm SO}^R = 6 \quad w_{\rm SO}^R = 5.62 \\ J_{\rm SO}^{(R1)} = 81.1 \quad \eta_{\rm SO}^R = 0.0407 \\ J_{\rm SO}^{(R2)} = 58.7 \quad A = 18.7 \end{cases}$
Imaginary Spin-orbit	$J_{\rm SO}^I(E) = \begin{cases} 0 & \text{for } E \leqslant 50 \text{ MeV} \\ J_{\rm SO}^I \frac{E^2}{E^2+{w_{\rm SO}^I}^2} & \text{for } E \geqslant 50 \text{ MeV}. \end{cases}$	$\left\{ J_{\rm SO}^{(I)} = -19.2 \quad w_{\rm SO}^I = 365 \right.$

[a] $J_R^{(2)}$, $J_{\rm IV}^{(2)}$, $J_{\rm IS}^{(2)}$, and $J_{\rm SO}^{(2)}$ values can be obtained from equating at the boundary values.

up to 200 MeV/nucleon as shown in Fig. 4(b). Therefore, we modify the Fermi parametrization formula to include the J_I decreasing after it reaches the maximum. The parametrizations and their best-fit parameters of the imaginary volume integrals are shown in Table III.

For the imaginary spin-orbit potential, the $J_{\rm SO}^I$ values are zero at low energies up to 50 MeV/nucleons, then it begin in its growing as shown in Fig. 4(c). Brieva and Rook predict that the imaginary part of the spin-orbit potential is of opposite sign to the real part, in agreement with our results and with most phenomenological analyses at intermediate energies. The functional form of Brown and Rho [94] that was successfully applied in Refs. [7,8,13] is used for $J_{\rm SO}^I$ in the present work.

The volume integrals parametrizations and their best-fitted parameters are shown in Table III for J_R, $J_{\rm IV}$, $J_{\rm IS}$, $J_{\rm SO}^R$, and $J_{\rm SO}^I$. The calculated volume integrals of the best-fit OPs for $p + {}^{9}$Be elastic scattering and their parameterized ones as functions of energy are shown in Figs. 4(a)–4(c). It is shown that these parametrization formulas fit the calculated volume integrals well.

In general, we can divide the energy range into three regions.

Region I. At low energies, the volume integrals of the real, imaginary, and real spin-orbit OPs increase with energy up to maximum values at definite energies (namely, E_R, $E_{\rm IV}$, $E_{\rm IS}$, $E_{\rm SO}^R$) for real, volume imaginary, surface imaginary, and real spin-orbit OPs. The increasing of the volume integrals at low energies is described by the rise parameters w_i where $i = R$, IV, IS, SO. In some cases, E_R and $E_{\rm SO}^R$ cannot be determined because there are no further data at low energies. Then, it can be neglected and the exponential-decay terms of $J_{\rm R}$ and $J_{\rm SO}^R$ are only considered. In addition, $J_{\rm SO}^I$ values are zero in this region. Generally, at low energies, the energy dependencies of the volume integrals are similar to the well-known threshold anomalies, which are caused by the rapid changes in the absorption as the inelastic channels open up near the Coulomb barrier [2].

Region II. At energies up to 200 MeV/nucleon, the volume integrals after reach the maximum values, they decrease with energy. The real and spin-orbit volume integrals are decreased exponentially whereas the imaginary volume integrals decrease slowly and linearly with energy. The decay parameters are denoted by η_R, $\eta_{\rm IV}^{(1)}$, $\eta_{\rm IS}^{(1)}$, $\eta_{\rm SO}^R$ for real, volume imaginary, surface imaginary, and real spin-orbit OPs, respectively. In this region, the negative $J_{\rm SO}^I$ values begin to increases with energies.

Region III. At high energies those larger than 200 MeV/nucleon. In this region, the volume integrals of the real central and spin-orbit potentials are approximately saturated whereas the imaginary volume integrals increase rapidly and linearly with increasing of energy up to 1000 MeV/nucleon. The rising parameter of J_I is denoted by $\eta_I^{(2)}$. In addition, in this region, the negative $J_{\rm SO}^I$ values continue in increasing with energy. It is useful to mention that for the elastic scattering of protons with bombarding energies near 200 MeV, the data need stronger imaginary part with wine-bottle-bottom shape for the real part [5].

C. Local *E*-dependent microscopic nucleon-nucleus OP

From the energy parametrization of the volume integrals, we can present an energy-dependent microscopic OP which depends only on the single-folding model. To construct energy-dependent microscopic OP (43), the energy dependence factors or the parameterized N-factors [$N_R(E)$, $N_{\rm IV}(E)$,

$N_{\rm IS}(E)$, $N^R_{\rm SO}(E)$, $N^I_{\rm SO}(E)$] can be determined by the equations (42) where the parameterized volume integrals as functions of energy are given in Table III and the volume integrals of the original potentials without normalization are given in Eqs. (40).

Then, the real, volume imaginary, surface imaginary, real and imaginary spin-orbit potentials can be rewritten as energy-dependent potentials as follows:

$$
\begin{aligned}
V(r,E) &= N_R(E)V_F(r) = \frac{J_R(E)}{J(V_F)}V_F(r)\\
W_v(r,E) &= N_{\rm IV}(E)W_H(r) = \frac{J_{\rm IV}(E)}{J(W_H)}W_H(r)\\
W_s(r,E) &= -N_{\rm IS}(E)r\frac{dW_H(r)}{dr} = \frac{J_{\rm IS}(E)}{J(rdW_H/dr)}r\frac{dW_H(r)}{dr}\\
V_{\rm SO}(r,E) &= N^R_{\rm SO}(E)V_{\rm LS}(r) = \frac{J^R_{\rm SO}(E)}{J(V_{\rm LS})}V_{\rm LS}(r)\\
W_{\rm SO}(r,E) &= N^I_{\rm SO}(E)V_{\rm LS}(r) = \frac{J^I_{\rm SO}(E)}{J(V_{\rm LS})}V_{\rm LS}(r),
\end{aligned}
\tag{44}
$$

and the total E-dependent microscopic OP for nucleon-nucleus scattering, $U_{\rm OP}(r,E)$ [Eq. (43)], can be rewritten as

$$
\begin{aligned}
U_{\rm OP}(r,E) = {} & \frac{J_R(E)}{J(V_F)}V_F(r) + i\frac{J_{\rm IV}(E)}{J(W_H)}W_H(r)\\
& - i\frac{J_{\rm IS}(E)}{J(-rdW_H/dr)}r\frac{d}{dr}W_H(r)\\
& + \left[\frac{J^R_{\rm SO}(E)}{J(V_{\rm LS})} + i\frac{J^I_{\rm SO}(E)}{J(V_{\rm LS})}\right]V_{\rm LS}(r)\mathbf{L}.\sigma.
\end{aligned}
\tag{45}
$$

This local energy-dependent OP (45) can be used to reproduce the scattering data of the $p+{}^9$Be reactions at a wide energy range that covers from 1–1000 MeV/nucleon. In addition, their energy dependence forms and behaviors can help us to obtain the correct energy and mass dependencies of the folding OPs. So, more studies are needed to check the ability of this hybrid microscopic OP to analyze the nucleon-nucleus scattering at intermediate and heavy nuclei. If it is successful then it can be used to construct a global microscopic nucleon-nucleus OP, which can be used in analyzing the scattering data at large ranges of nuclei and energies; also it can be used in predicting the data of the reactions for energies and exotic nuclei at which no experimental data are available.

Figure 4(d) presents the parameterized N factors of the OP parts in comparison with the corresponding best-fit ones. These factors can be obtained from Eqs. (42) using the values in Eqs. (40) and Table III. Also, they can be fitted and parameterized directly from the best-fit N factors. It is clear that the energy dependencies of these parameterized N factors are rapidly changed at low energies corresponding to what may be the rapid changes in the absorption as the inelastic channels open up near the Coulomb barrier [2]. On other hand, they are changed slowly at high energies. One can shown that $N_R(E)$ and $N^R_{\rm SO}(E)$ are decreased exponentially with energy increasing whereas $N_{\rm IV}(E)$ and $N_{\rm IS}(E)$ seem to increase with $\ln E$. In addition, the corresponding total imaginary normalization factor $N_{\rm I}(E)$ in the case of using of the volume imaginary term only (without surface part) can be obtained from Eqs. (40) as $N_{\rm I}(E) = N_{\rm IV}(E) + 3N_{\rm IS}(E)$. This explains why the values of $N_{\rm IV}(E)$ and $N_{\rm IS}(E)$ are still small and far from unity even at the considered intermediate and high energies.

Early, the original M3Y-Paris NN interaction is multiplied by an energy-dependent factor $g(E) \simeq 1 - 0.003E$ in order to reproduce the data of nucleus-nucleus scattering at energies up to 100 MeV/nucleon [22,27,31] where E is the bombarding energy per nucleon. In the present work, $N_R(E)$ can be obtained from Eqs. (42) using the values in Eqs. (40) and Table III as $N_R(E) \sim \exp(-0.0068E)$.

Generally, in the folding potential, the density gives the geometry information and the NN interaction gives the depth and shape of the potential. Therefore, these $N(E)$ can be included in the original NN interaction as an energy dependence term. But we need to know the mass dependence of this term, so we need more studies for nucleon-nucleus scattering for more scattered nuclei at a wide energy range.

IV. SUMMARY AND CONCLUSIONS

The proton elastic scattering of ^{9}Be at energies from few MeV/nucleon to 1000 MeV/nucleon was analyzed by the optical model with partial wave expansion method. The real OP was taken within single-folding model by use of the density- and isospin-dependent M3Y-Paris NN interaction and GFMC density of ^{9}Be nucleus. The spin-orbit part was presented by the Brieva-Rook model using the two-body spin-orbit M3Y-Paris NN interaction. The volume and surface imaginary parts of OP were given by the high-energy approximation model, which folds the NN-scattering amplitude and the density of the scattered nucleus. This hybrid OP was used within the optical model to analyze the basic scattering data (angular distributions for elastic-scattering cross sections and analyzing powers, reaction and total cross sections).

A comparison between the derivative spin-orbit, which was taken by the derivative of the real central OP and the Brieva-Rook spin-orbit potential showed that the derivative spin-orbit is not suitable for energies larger than 100 MeV/nucleon.

Another comparison between OP with and without surface imaginary part was done. This comparison showed that using of OP without surface imaginary part gives results that do not agree with the data at energies above 100 MeV/nucleon where some minima appear in the calculated angular distribution of the elastic-scattering cross sections. A new behavior of the imaginary potential and their volume integrals was found at scattering at high energies. Considering the surface as well as volume imaginary potential at these high energies filled the minima at the angular distributions and gave good agreement with the cross-section data. Furthermore, the σ_R and $\sigma_{\rm tot}$ values obtained using the surface part are larger than those without surface term and give the best agreement with the data of the high-energy scattering.

Generally, including the surface contribution to the scattering OP at the whole energy range give results in good quality agreement with the experimental data of the differential cross section of elastic scattering as well as reaction and total cross sections over all energy ranges. The analyzing power

data are fitted well at low energies. At energies larger than 50 MeV/nucleon, the A_y structure at forward scattering angles are fitted well but the calculated A_y at the backward scattering angles are not in a good agreement with the data.

The volume integrals have systematic behaviors for the energy dependence. At low energies, the J_R, $J_{\rm IV}$, $J_{\rm IS}$, and $J^R_{\rm SO}$ increase with increasing energy until they reach a maximum at definite values of energy. Thereafter, with increasing incident energy, the J_R and $J^R_{\rm SO}$ decrease exponentially and they saturate at energies larger than 200 MeV/nucleon. On the other hand, after they reach maximum values, the $J_{\rm IV}$ and $J_{\rm IS}$ decrease linearly with a small slope until 200 MeV/nucleon. Then, they increase linearly and rapidly again with energy up to 1 GeV/nucleon.

The energy dependencies of the OP parts were determined as functions of energy. They were calculated from the parametrization of the volume integrals of the best-fit OPs. The new behaviors of volume and surface imaginary OPs at high energies need more studies for nucleon elastic scattering at other nuclei.

ACKNOWLEDGMENTS

I would like to present my thanks and appreciation to the Institute of International Education (IIE) for granting the Rescue Scholar Fund Program Award (IIE-SRF fellowship) that supports, arranges and funds fellowships for threatened and displaced scholars at partnering higher education institutions worldwide.

[1] P. E. Hodgson, Rep. Prpg. Phys. **34**, 765 (1971).
[2] M. E. Brandan and G. R. Satchler, Phys. Rep. **285**, 143 (1997).
[3] G. R. Satchler and W. G. Love, Phys. Rep. **55**, 183 (1979).
[4] D. T. Khoa, G. R. Satchler, and W. von Oertzen, Phys. Rev. C **56**, 954 (1997).
[5] G. R. Satchler, Nucl. Phys. A **394**, 349 (1983).
[6] D. T. Khoa, G. R. Satchler, and W. von Oertzen, Phys. Rev. C **51**, 2069 (1995).
[7] X. Li and Chonghai Cai, Nucl. Phys. A **801**, 43 (2008).
[8] A. J. Koning and J. P. Delaroche, Nucl. Phys. A **713**, 231 (2003).
[9] O. V. Bespalova, E. A. Romanovsky, and T. I. Spasskaya, J. Phys. G: Nucl. Part. Phys. **29**, 1193 (2003).
[10] F. D. Becchetti and G. W. Greenlees, Phys. Rev. **182**, 1190 (1969).
[11] C. M. Perey and F. G. Perey, At. Data Nucl. Data Tables **17**, 1 (1976).
[12] R. L. Varner, W. J. Thompson, T. L. McAbee, E. J. Ludwig, and T. B. Clegg, Phys. Rep. **201**, 57 (1991).
[13] B. Morillon and P. Romain, Phys. Rev. C **70**, 014601 (2004); **76**, 044601 (2007).
[14] J. S. Petler, M. S. Islam, R. W. Finlay, and F. S. Dietrich, Phys. Rev. C **32**, 673 (1985).
[15] B. A. Watson, P. P. Singh, and R. E. Segel, Phys. Rev. **182**, 977 (1969).
[16] M. Y. H. Farag, E. H. Esmael, and H. M. Maridi, Eur. J. Phys. A **48**, 154 (2012).
[17] M. Y. H. Farag, E. H. Esmael, and H. M. Maridi, Phys. Rev. C **88**, 064602 (2013).
[18] M. Y. H. Farag, E. H. Esmael, and H. M. Maridi, Eur. J. Phys. A **50**, 106 (2014).
[19] M. Y. H. Farag, E. H. Esmael, and H. M. Maridi, Phys. Rev. C **90**, 034615 (2014).
[20] H. M. Maridi, M. Y. H. Farag, and E. H. Esmael, in *Proceedings of the Fifth Saudi International Meeting on Frontiers of Physics (SIMFP2016)*, edited by A. Al-Kamli, N. Can, G. O. Souadi, M. Fadhali, A. Mahdy, and M. Mahgoub, AIP Conf. Proc. No. 1742 (AIP, New York, 2016), p. 030011.
[21] H. M. Maridi, in *The Sixth Saudi International Meeting on Frontiers of Physics 2018 (SIMFP2018)*, edited by A. Al-Kamli, G. O. Souadi, J. Hakami, N. Can, A. Mahdy, M. Mahgoub, and Zaka-ul-Islam Mujahid, AIP Conf. Proc. No. 1976 (AIP, New York, 2018), p. 020004.
[22] D. T. Khoa, E. Khan, G. Colò, and N. Van Giai, Nucl. Phys. A **706**, 61 (2002).
[23] F. A. Brieva and J. R. Rook, Nucl. Phys. A **297**, 206 (1978).
[24] P. Shukla, Phys. Rev. C **67**, 054607 (2003).
[25] V. K. Lukyanov, E. V. Zemlyanaya, and K. V. Lukyanov, Phys. At. Nucl. **69**, 240 (2006).
[26] K. V. Lukyanov, V. K. Lukyanov, E. V. Zemlyanaya, A. N. Antonov, and M. K. Gaidarov, Eur. J. Phys. A **33**, 389 (2007).
[27] D. T. Khoa, W. von Oertzen, and A. A. Ogloblin, Nucl. Phys. A **602**, 98 (1996).
[28] B. Sinha, Phys. Rep. **20**, 1 (1975).
[29] N. Anantaraman, H. Toki, and G. F. Bertsch, Nucl. Phys. A **398**, 269 (1983).
[30] G. Bertsch, J. Borysowicz, H. McManus, and W. G. Love, Nucl. Phys. A **284**, 399 (1977).
[31] D. T. Khoa and W. von Oertzen, Phys. Lett. B **304**, 8 (1993).
[32] Steven C. Pieper, K. Varga, and R. B. Wiringa, Phys. Rev. C **66**, 044310 (2002).
[33] X. Campi and A. Bouyssy, Phys. Lett. B **73**, 263 (1978).
[34] P. Ring and P. Schuck, *The Nuclear Many-Body Problem* (Springer-Verlag, New York, 1980), p. 542.
[35] Dao T. Khoa, W. von Oertzen, and H. G. Bohlen, Phys. Rev. C **49**, 1652 (1994).
[36] R. J. Glauber, in *Lectures in Theoretical Physics*, edited by W. E. Brittin and G. L. Dunham (Interscience, New York, 1959), Vol. 1, p. 315.
[37] V. K. Lukyanov, E. V. Zemlyanaya, K. V. Lukyanov, D. N. Kadrev, A. N. Antonov, M. K. Gaidarov, and S. E. Massen, Phys. Rev. C **80**, 024609 (2009).
[38] S. Kumar and Y. G. Ma, Phys. Rev. C **91**, 034612 (2015).
[39] V. K. Lukyanov, D. N. Kadrev, E. V. Zemlyanaya, K. Spasova, K. V. Lukyanov, A. N. Antonov, and M. K. Gaidarov, Phys. Rev. C **91**, 034606 (2015).
[40] P. Shukla, arXiv:nucl-th/0112039.
[41] S. K. Charagi and S. K. Gupta, Phys. Rev. C **41**, 1610 (1990); **46**, 1982 (1992).
[42] H. A. Enge, *Introduction to Nuclear Physics* (Addison-Wesley, Reading, 1966).
[43] N. Keeley, N. Alamanos, K. W. Kemper, and K. Rusek, Prog. Part. Nucl. Phys. **63**, 396 (2009).
[44] S. A. Fayans, O. M. Knyazkov, I. N. Kuchtina, Yu. E. Penionzhkevich, and N. K. Skobelev, Phys. Lett. B **357**, 509 (1995).

[45] V. K. Lukyanov, D. N. Kadrev, E. V. Zemlyanaya, A. N. Antonov, K. V. Lukyanov, and M. K. Gaidarov, Phys. Rev. C **82**, 024604 (2010).

[46] M. Y. M. Hassan, M. Y. H. Farag, E. H. Esmael, and H. M. Maridi, Phys. Rev. C **79**, 014612 (2009).

[47] M. Y. M. Hassan, M. Y. H. Farag, E. H. Esmael, and H. M. Maridi, Phys. Rev. C **79**, 064608 (2009).

[48] K. V. Lukyanov, I. N. Kukhtina, V. K. Lukyanov, Yu. E. Penionzhkevich, Yu. G. Sobolev, and E. V. Zemlyanaya, in *International Symposium on Exotic Nuclei*, edited by Yu. E. Penionzhkevich and E. A. Cherepanov, AIP Conf. Proc. No. 912 (AIP, New York, 2007), p. 170.

[49] R. S. Mackintosh and A. M. Kobos, J. Phys. G: Nucl. Phys. **4**, L135 (1978).

[50] E. Bauge, J. P. Delaroche, and M. Girod, Phys. Rev. C **58**, 1118 (1998).

[51] L. J. de Bever *et al.*, Nucl. Phys. A **579**, 13 (1994).

[52] I. Abdul-Jalil and D. F. Jackson, J. Phys. G: Nucl. Phys. **5**, 1699 (1979).

[53] D. F. Jackson and I. Abdul-Jalil, J. Phys. G: Nucl. Phys. **6**, 481 (1980).

[54] R. A. Hutcheon *et al.*, Nucl. Phys. A **483**, 429 (1988).

[55] R. R. Sheerbaum, Nucl. Phys. A **257**, 77 (1976).

[56] W. Haider, Syed Rafi, J. R. Rook, and Y. K. Gambhir, Phys. Rev. C **93**, 054615 (2016).

[57] D. H. Loyd and W. Haeberli, Nucl. Phys. A **148**, 236 (1970).

[58] F. W. Bingham, M. K. Brussel, and J. D. Steben, Nucl. Phys. **55**, 265 (1964).

[59] H. J. Votava, T. B. Clegg, E. J. Ludwig, and W. J. Thompson, Nucl. Phys. A **204**, 529 (1973).

[60] D. G. Montague, R. K. Cole, P. S. Lewis, C. N. Waddell, and D. L. Hendrie, Nucl. Phys. A **199**, 433 (1973).

[61] E. Fabrici, S. Micheletti, M. Pignanelli, F. G. Resmini, R. De Leo, G. D'Erasmo, and A. Pantaleo, Phys. Rev. C **21**, 844 (1980).

[62] J. W. Verba, H. Willmes, R. F. Carlson, I. Slaus, J. Reginald Richardson, and E. L. Petersen, Phys. Rev. **153**, 1127 (1967).

[63] N. M. Clarke, E. J. Burge, D. A. Smith, and J. C. Dore, Nucl. Phys. A **157**, 145 (1970).

[64] H. Seifert, Ph.D. thesis, University of Maryland, 1990 (unpublished).

[65] J. J. Kelly, Phys. Rev. C **38**, 1490 (1988).

[66] P. G. Roos and N. S. Wall, Phys. Rev. **140**, B1237 (1965).

[67] S. Dixit, W. Bertozzi, T. N. Buti, J. M. Finn, F. W. Hersman, C. E. Hyde-Wright, M. V. Hynes, M. A. Kovash, B. E. Norum, J. J. Kelly, A. D. Bacher, G. T. Emery, C. C. Foster, W. P. Jones, D. W. Miller, B. L. Berman, and D. J. Millener, Phys. Rev. C **43**, 1758 (1991).

[68] H. Seifert, J. J. Kelly, A. E. Feldman, B. S. Flanders, M. A. Khandaker, Q. Chen, A. D. Bacher, G. P. A. Berg, E. J. Stephenson, P. Karen, B. E. Norum, P. Welch, and A. Scott, Phys. Rev. C **47**, 1615 (1993).

[69] G. Roy *et al.*, Nucl. Phys. A **442**, 686 (1985).

[70] J. J. Kelly, A. E. Feldman, B. S. Flanders, H. Seifert, D. Lopiano, B. Aas, A. Azizi, G. Igo, G. Weston, C. Whitten, A. Wong, M. V. Hynes, J. McClelland, W. Bertozzi, J. M. Finn, C. E. Hyde-Wright, R. W. Lourie, P. E. Ulmer, B. E. Norum, and B. L. Berman, Phys. Rev. C **43**, 1272 (1991).

[71] B. S. Flanders, J. J. Kelly, H. Seifert, D. Lopiano, B. Aas, A. Azizi, G. Igo, G. Weston, C. Whitten, A. Wong, M. V. Hynes, J. McClelland, W. Bertozzi, J. M. Finn, C. E. Hyde-Wright, R. W. Lourie, B. E. Norum, P. Ulmer, and B. L. Berman, Phys. Rev. C **43**, 2103 (1991).

[72] G. D. Alkhazov, S. L. Belostotskij, A. A. Vorob'ev, O. A. Domchenkov, Yu. V. Dotsenko, N. P. Kuropatkin, and V. N. Nikulin, Yad. Fiz. **42**, 8 (1985).

[73] K. Fukunaga, J. Phys. Soc. Jpn. **20**, 1 (1965).

[74] L. Rosen, J. E. Brolley, Jr., M. L. Gursky, and L. Stewart, Phys. Rev. **124**, 199 (1961).

[75] L. Rosen, J. E. Brolley, Jr., and L. Stewart, Phys. Rev. **121**, 1423 (1961).

[76] D. J. Baugh, J. A. R. Griffith, and S. Roman, Nucl. Phys. **83**, 481 (1966).

[77] D. L. Watson, J. Lowe, J. C. Dore, R. M. Craig, and D. J. Baugh, Nucl. Phys. A **92**, 193 (1967).

[78] T. A. Cahill, J. Reginald Richardson, and R. P. Haddock, Phys. Rev. **144**, 932 (1966).

[79] G. S. Mani, D. Jacques, and A. D. B. Dix, Nucl. Phys. A **165**, 145 (1971).

[80] D. J. Steinberg, J. N. Palmieri, aand A. M. Cormack, Nucl. Phys. **56**, 46 (1964).

[81] A. Johansson, G. Tibell, and P. Hillman, Nucl. Phys. **11**, 540 (1959).

[82] O. Chamberlain, E. Segre, R. D. Tripp, C. Wiegand, and T. Ypsilantis, Phys. Rev. **102**, 1659 (1956).

[83] R. F. Carlson, At. Data Nucl. Data Tables **63**, 93 (1996).

[84] A. de Vismes *et al.*, Nucl. Phys. A **706**, 295 (2002).

[85] N. M. Clarke (1994, unpublished).

[86] F. G. Perey and B. Buck, Nucl. Phys. **32**, 353 (1962).

[87] W. T. H. Van Oers and H. Haw, Phys. Lett. B **45**, 227 (1973).

[88] A. Nadasen, S. Balaji, J. Brace, K. A. G. Rao, P. G. Roos, P. Schwandt, and J. T. Ndefru, Phys. Rev. C **66**, 064605 (2002).

[89] P. Mohr, Phys. Rev. C **61**, 045802 (2000).

[90] P. Demetriou, C. Grama, and S. Goriely, Nucl. Phys. A **707**, 253 (2002).

[91] U. Atzrott, P. Mohr, H. Abele, C. Hillenmayer, and G. Staudt, Phys. Rev. C **53**, 1336 (1996).

[92] E. Somorjai, Zs. Fülöp, Á. Z. Kiss, C. E. Rolfs, H. P. Trautvetter, U. Greife, M. Junker, S. Goriely, M. Arnould, M. Rayet, T. Rauscher, and H. Oberhummer, Astron. Astrophys. **333**, 1112 (1998).

[93] Zs. Fülöp, Gy. Gyürky, Z. Máté, E. Somorjai, L. Zolnai, D. Galaviz, M. Babilon, P. Mohr, A. Zilges, T. Rauscher, H. Oberhummer, and G. Staudt, Phys. Rev. C **64**, 065805 (2001).

[94] G. E. Brown and M. Rho, Nucl. Phys. A **372**, 397 (1981).

[95] J. P. Jeukenne and C. Mahaux, Nucl. Phys. A **394**, 445 (1983).